ACS OMEGA

Article

Cite This: ACS Omega 2018, 3, 17466−17473

http://pubs.acs.org/journal/acsodf

Graphene-like MoS_2 Nanosheets on Carbon Fabrics as High-Performance Binder-free Electrodes for Supercapacitors and Li-Ion Batteries

Hong Yin,[†,∥] Yuan Liu,[†,∥] Neng Yu,[‡] Hong-Qing Qu,[†] Zhitian Liu,[§] Renzhi Jiang,[†] Chong Li,*[,†] and Ming-Qiang Zhu*[,†]

[†]Wuhan National Laboratory for Optoelectronics (WNLO), School of Optics and Electronic Information, Huazhong University of Science and Technology, Wuhan 430074, China

[‡]Jiangxi Province Key Laboratory of Polymer Micro/Nano Manufacturing and Devices, School of Chemistry, Biology and Materials Science, East China University of Technology, Nanchang 330013, China

[§]School of Materials Science & Technology, Wuhan Institute of Technology, Wuhan 4302054, China

Supporting Information

ABSTRACT: Two-dimensional layer-structure materials are now of great interest in energy storage devices, owing to their graphene-like structure and high theoretical capacity. Herein, graphene-like molybdenum disulfide (MoS_2) nanosheets were uniformly grown on carbon fabrics by using a hydrothermal method. They were evaluated as binder-free electrodes for Li-ion batteries (LIBs) and supercapacitors. As expected, long cycling life and high capacity/capacitance are achieved. When used as self-standing electrodes for LIBs, they deliver a high area capacity of ∼0.5 mAh/cm^2 even after 400 cycles and remarkable rate capability in the charge/discharge potential range of 1−3 V. In addition, a three-dimensional integrated electrode of the MoS_2 nanosheet exhibits a high capacitance of 103.5 mF/cm^2 and long cycling stability up to at least 15 000 cycles at a current density of 3 mA/cm^2 for supercapacitors. The great cycling stability of MoS_2 in supercapacitors is promising in the enhancement of cycling stability through their integration with other materials as alternatives to graphene in some special fields.

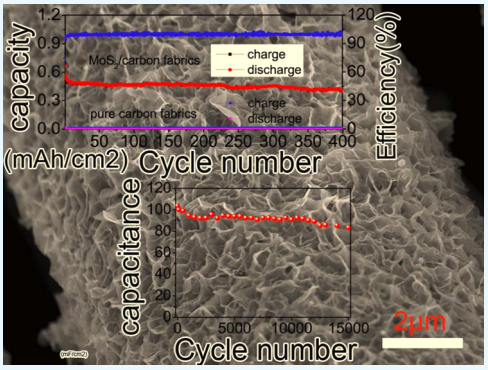

1. INTRODUCTION

Nowadays, energy storage devices have attracted worldwide attention due to their vital roles as dominant mobile power sources for a range of applications, such as mobile devices, new-energy vehicles, and smart devices.[1−4] To develop high-performance electrode materials for lithium-ion batteries (LIBs) and supercapacitors (SCs), metal oxide nanostructures with high specific capacity/capacitance, typically 2−3 times higher than that of the carbonous materials, have attracted much attention.[5−8] However, their poor cycling stability leads to worse electrochemical performance which cannot satisfy the practical applications. Therefore, developing electrode materials with long cycle lives is still an urgent mission.

Since graphene was discovered in 2004, many other two-dimensional (2D) layer-structure materials have also regained research interest.[9−15] So far, among those two-dimensional (2D) layer-structure materials, molybdenum disulfide (MoS_2) has played a significant role, which has been extensively studied for many applications such as photodetectors, water treatments, memorizers, and especially for SCs and LIBs.[16−19] However, when evaluating as an electrode material for Li-ion batteries, due to the large volume change during the charging/discharging cycles, the conductivity is low and the structure is destroyed, resulting in faster capacity decay. To resolve this problem, a feasible way is to composite with other materials which have excellent electronic conductivity, such as graphene, carbon nanotubes, etc.[20−23] Another approach is to increase the interlayer distance of MoS_2, which will also introduce voids and defects into MoS_2 to increase its lithium ion storage capacity. The third way is to design binder-free electrodes.

Compared to traditional binder-enriched materials, the self-standing electrode does not have any additional current collector or binder, which leads to high-speed electron transport and ion diffusion. Therefore, the binder-free electrode can effectively enhance the electrochemical performance of active materials. In recent years, specific mechanical and electronic properties of three-dimensional (3D) flexible binder-free energy storage devices have attracted great attention for the next generation, such as LIBs and SCs.[24−27] For instance, the synthesis of graded 3D $ZnCo_2O_4$ nanowire array/carbonless cloth binder LIB integrated electrode is reported with high reversible capacity and good cycling

Received: September 20, 2018
Accepted: November 23, 2018
Published: December 17, 2018

DOI: 10.1021/acsomega.8b02446
ACS Omega 2018, 3, 17466−17473

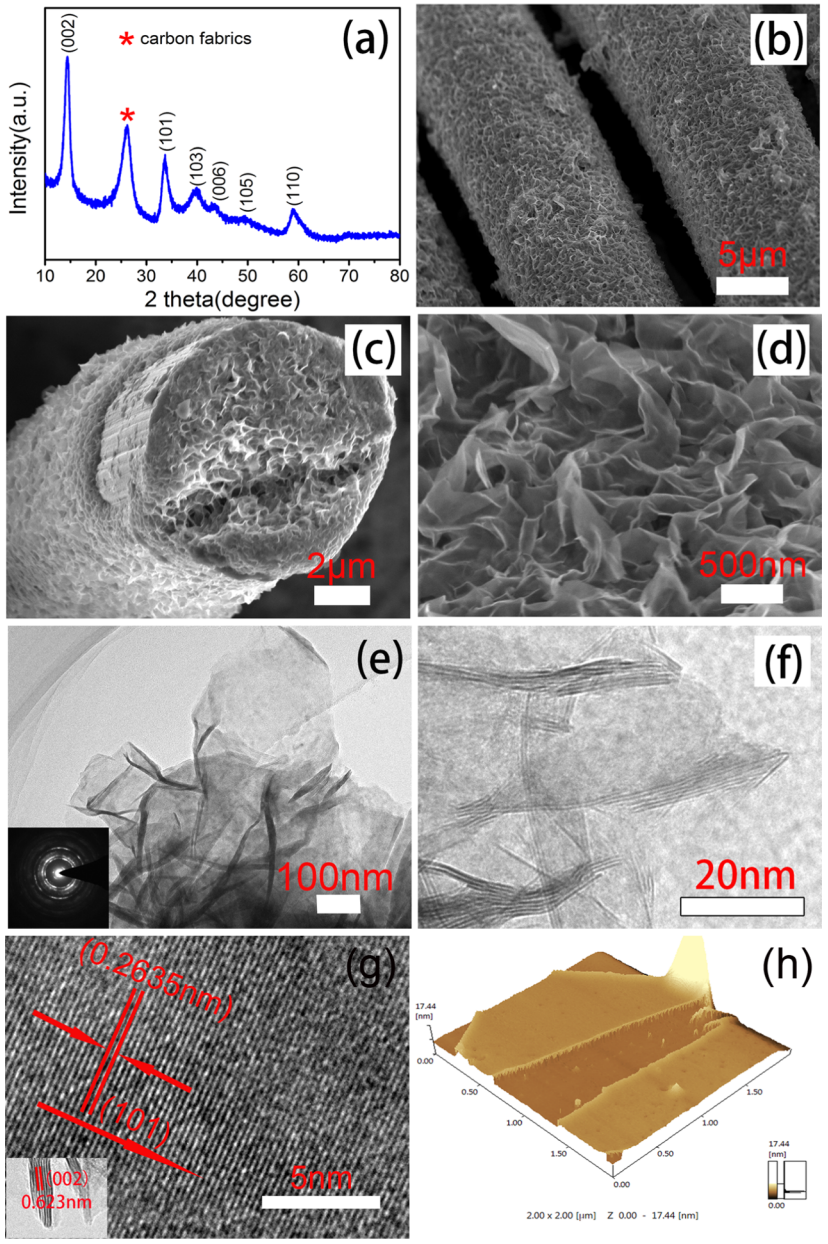

Figure 1. (a) XRD pattern, (b–d) SEM images of graphene-like MoS_2 nanosheets on carbon fabrics. (e, f) TEM images of the MoS_2 nanosheets and the inset (e) shows the corresponding SAED pattern. (g) HR-TEM image of MoS_2 nanosheets. (h) Three-dimensional AFM image of MoS_2 nanosheets.

performance.[28] Cheng et al. also developed an LTO/graphene foam self-standing electrode with excellent electrochemical properties.[29] SCs and LIBs have many common features in improving the electrochemical properties of active materials despite their different charge storage mechanisms. The rationally designed binder-free electrodes are among them. Very recently, the electrodes based on $NiCo_2O_4$ nanowire arrays on carbon textiles synthesized by Zhang et al. exhibited high reversible capacity/capacitance and excellent cycling ability for LIBs and SCs.[30] Oxygen-deficient Fe_2O_3 nanorods on carbon fabrics were synthesized by Lu et al., and high capacitance and excellent cycling stability are achieved when used as anodes for SCs.[31]

In previous reports, many kinds of composites based on MoS_2 were synthesized to enhance the cycling stability of MoS_2. Recently, to get a more excellent anode material for LIBs, hierarchical MoS_2 nanosheets/activated carbon fiber cloth and three-dimensional hierarchical MoS_2 nano-array/carbon cloth were synthesized and evaluated. However, the galvanostatic charging and discharging tests were performed at a potential ranging from 5 mV to 3 V and 1 mV to 3 V, respectively, and the cycling performance is not so good. Moreover, when the charge/discharge voltage was below 1 V, the carbon cloth and active carbon fiber can contribute a great deal of the capacity to the whole electrode, which results in the calculated capacity of active materials higher than real.[32−34] At the same time, MoS_2-based SCs are mainly binder-enriched. According to previous reports, MoS_2 can be widely used in almost all commonly used electrolytes, because of the relative stability of MoS_2 in acid, neutral, and alkaline aqueous solutions. When used in alkaline aqueous solution, some researchers choose Ni foam as the current collector. However,

DOI: 10.1021/acsomega.8b02446
ACS Omega 2018, 3, 17466−17473

the Ni foam can easily form NiO on the surface and has a great influence on the measurement of capacitor properties, which may result in error and exaggerated capacitance, especially when a little amount of electrode-active materials are used for the measurements.[35−37] To avoid the above problem, carbon fabrics used as the current collector of the SC electrode may be a good choice, which can reflect the SC properties of active materials more accurately.

In this work, graphene-like MoS_2 nanosheets on carbon fabrics are successfully synthesized in a typical and easy hydrothermal method and directly used as self-standing electrodes for LIBs and SCs. When evaluated as anodes of LIBs, this kind of integrated electrode showed high regional capacity, long cycling stability, and excellent rate performance in a galvanostatic charging and discharging potential window ranging from 1 to 3 V. When evaluated as electrodes for SCs, the as-synthesized integrated electrodes exhibited long cycling stability until 15 000 cycles with a capacitance fading of only 19.4% in a two-electrode coin cell configuration, when the current density is 3 mA/cm^2.

2. RESULTS AND DISCUSSION

2.1. Morphologies and Structural Analysis. The graphene-like MoS_2 nanosheets grown in carbon fabrics were synthesized via an easy hydrothermal method. Figure 1a shows the X-ray diffraction (XRD) pattern of the MoS_2 nanosheets. The pattern can be well indexed to hexagonal MoS_2 (JCPDS card no. 73-1508). The peak located at 2θ = 26° is a typical diffraction caused by carbon fabrics. The other peaks located at 2θ = 14.39, 33.62, 39.65, 44.14, 49.87, and 58.56° can be assigned to the (002), (101), (103), (006), (105), and (110) planes of the hexagonal MoS_2 phase, respectively. Their morphologies were characterized through the use of field-emission scanning electron microscopy (FESEM) and FE-transmission electron microscopy (FE-TEM). Figure 1b shows the SEM image of the as-synthesized products, which were evenly coated high-density samples. The higher magnification of the SEM image shown in Figure 1d reveals that the samples on the carbon fabrics are graphene-like ultrathin nanosheet structures. To clearly observe the thickness of the sample on the carbon fabrics, the sectional view of the as-synthesized product is shown in Figure 1c. We can clearly estimate that the thickness of MoS_2 nanosheets coated on carbon fabrics was ca. 200−300 nm. Figure 1e shows the TEM image of the MoS_2 nanosheets which were scratched from the carbon fabrics, and we can clearly see a two-dimensional layer-structure, corresponding to the SEM images very well (Figure 1d). The selected-area electron diffraction (SAED) and high-resolution TEM (HR-TEM) analyses effectively indicate the polycrystalline texture of MoS_2 nanosheets (Figure 1e,g). The lattice fringes are visible, and the *d*-spacing of 0.2635 nm was computed to correspond well to the (101) lattice plane of the hexagonal MoS_2 nanosheet. The higher magnification image of MoS_2 nanosheets is shown in Figure 1f. We can observe a well-defined layered structure of MoS_2 nanosheets. The thickness of the MoS_2 nanosheet is about 2.5 nm, which was characterized by an atomic force microscope (AFM) in Figure 1h.

The detailed elemental composition and the valence states on the surface of MoS_2 nanosheets are further characterized by X-ray photoelectron spectroscopy (XPS). The investigated spectrum of the MoS_2/carbon fabrics (Figure 2a) shows the existence of Mo, S, C, and O elements. Figure 2b,c show the high-resolution XPS spectra of Mo 3d and S 2p obtained from

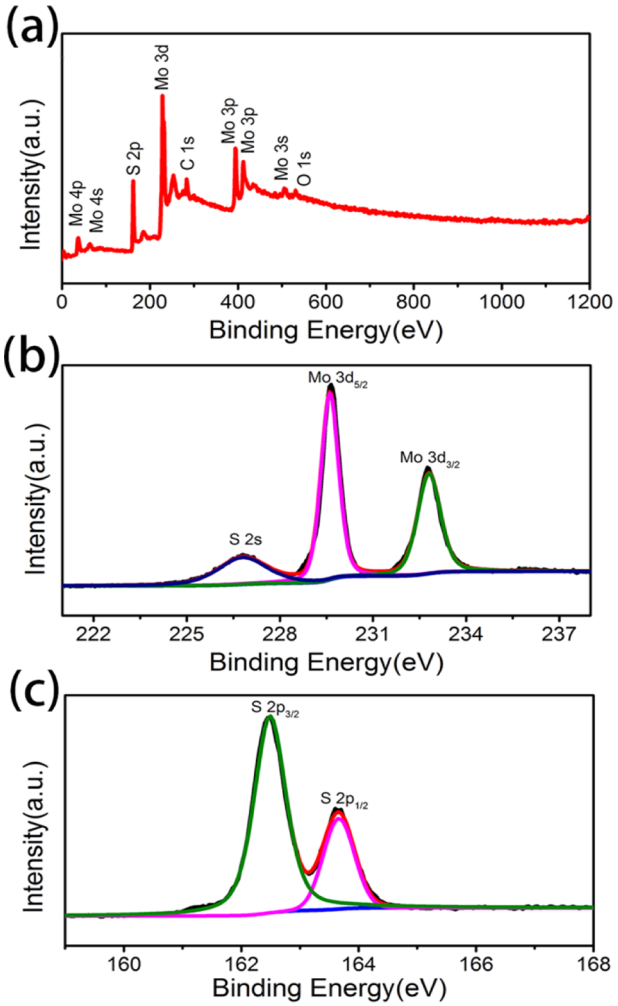

Figure 2. XPS spectra of graphene-like MoS_2 nanosheets on carbon fabrics. (a) Survey spectra and high-resolution spectra of (b) Mo 3d and S 2s, and (c) S 2p.

the MoS_2/carbon fabrics. The high-resolution Mo 3d peak (Figure 2b) shows two sub-peaks and a small peak at the binding energies of 229.6, 232.8, and 226.8 eV that correspond to the Mo $3d_{5/2}$, Mo $3d_{3/2}$, and S 2s states, respectively, indicating that molybdenum is in its Mo (IV) state. In Figure 2c, the peaks at the binding energies of 163.6 and 162.5 eV correspond to the S $2p_{1/2}$ and S $2p_{3/2}$ states, respectively. All of the binding energy values are well consistent with those reported for MoS_2.[38]

2.2. Li-Ion Battery Performance. Coin-type cell configuration was used to assess the energy storage properties of MoS_2/carbon fabrics for LIBs. The mass loading of MoS_2 nanosheets on carbon fabrics used for LIB tests is about 2.5−3 mg. MoS_2 nanosheet/carbon fabric as a cathode was compared with Li metal under the constant current circulation conditions under the potential window of 0.01−3 and 1−3 V at the current rate of 0.2 mA/cm^2 at room temperature. When the discharge potential was below 1 V, the carbon fabrics will react with Li metal, and this process is nearly irreversible. As a result, the Li metal will be wasted and lead to low Coulombic efficiency. Furthermore, the reduction peak of MoS_2 does not exist below 1 V. Therefore, we test the electrochemical performance of MoS_2/carbon fabrics at a potential ranging from 1 to 3 V. Figure S1 shows the charge/discharge profiles of

DOI: 10.1021/acsomega.8b02446
ACS Omega 2018, 3, 17466−17473

MoS_2/carbon fabrics and pure carbon fabrics for the 1st, 5th, and 60th, respectively. We can see that the pure carbon fabrics exhibit high area capacity (Figure S1b). The first-discharge reaction of MoS_2/carbon fabrics comprises mainly two regions. The first potential plateau at ∼1.1 V associated with the reaction of MoS_2 and Li^+ as in eq 1. The second plateau at ∼0.6 V is associated with the reduction of Mo^{4+} into the metallic Mo embedded into a cubic Li_2S matrix through the conversion process (eq 2) and the formation of a gel-like solid electrolyte interphase layer at the interface of the electrolyte and the electrode. In the charge profiles, the two plateaus at ∼1.7 and ∼2.3 V are associated with the oxidation of cubic Mo to hexagonal MoS_2 and dissociation oxidation of Li_2S to sulfur, respectively. In the second and subsequent discharge profiles, two potential plateaus at ∼1.8 and ∼1.15 V are associated with reduction of S to Li_2S and the formation of lithium intercalate of Li_xMoS_2, respectively.

$$MoS_2 + xLi^+ + xe^- \rightarrow Li_xMoS_2 \quad (1)$$

$$MoS_2 + 4Li^+ + 4e^- \rightarrow 2Li_2S + Mo \quad (2)$$

Considering that the main lithiation/delithiation reaction of MoS_2 is above 1 V after the first cathodic process, and the potential plateau is above 2 V, the capacity contribution below 1 V cannot be taken into consideration when assembled into full battery, then, we think that the galvanostatic charge/discharge tests of MoS_2/carbon fabrics performed at a potential ranging from 1 to 3 V are more suitable.

Figure 3a shows the charge/discharge profiles of MoS_2/carbon fabrics for the 1st, 20th, 100th, 300th, and 400th at the potential between 1 and 3 V, respectively. Because the reduction process (eq 2) may not occur in the first discharge process, the corresponding oxidation process may not exist either. The reaction mechanism can be changed when the potential window changed. According to Figure 3a, during the first discharge, a large plateau at about 1.25 V can be attributed to the reaction of MoS_2 and Li^+ as in eq 1. The reaction of eq 2 does not exist. In the first charge process, a large inconspicuous plateau between 1.5 and 2.5 V may be associated with the extraction of Li^+ from the Li_xMoS_2 lattice. In the subsequent cycles, only a simple insertion/extraction process occurs. It should be noted that the Li^+ intercalate potential of the first discharge process is lower than the subsequent cycles, which can be attributed to the different discharge depth resulting in the different Li^+ insertion potential. Figure 3b shows the cycling performance of MoS_2/carbon fabrics and pure carbon fabrics at a current density of 0.2 mA/cm^2 in the potential window between 1 and 3 V. Because the pure carbon fabrics contribute such little capacity to the whole electrode, the reaction of Li with carbon fabrics can be neglected. After 400 cycles, the MoS_2/carbon fabrics still hold a high reversible area capacity of 0.4 mAh/cm^2, about 80% capacity retention after the 1st cycle, compared to the cycling performance of MoS_2 carbon fabrics tested at a potential window from 0.01 to 3 V (Figure S2), which shows a capacity retention of only 63% in the 60th cycle after the 1st cycle. The enhanced cycling performance of MoS_2/carbon fabrics when tested at a potential ranging from 1 to 3 V can be attributed to two reasons. First, the depth of discharge can result in the easier destruction of the electrode. Second, the current collector taking part in the electrochemical reaction may result in the active materials peeling off from the current collectors and the capacity fading rapidly. To provide more direct evidence, the morphologies of

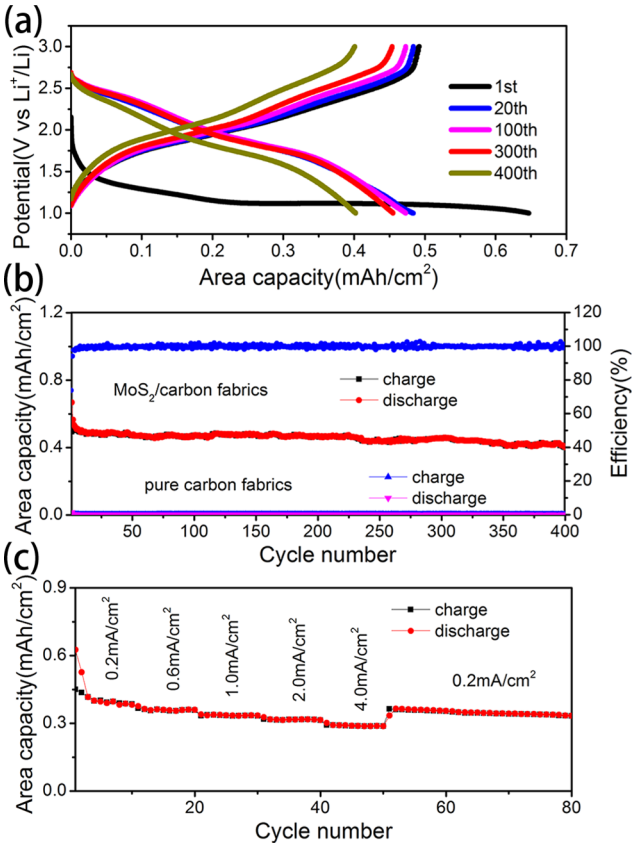

Figure 3. (a) Charge/discharge profiles, (b) cycling performance at 0.2 mA/cm^2 and (c) rate performance of MoS_2 carbon fabrics in the potential range of 1−3 V.

MoS_2/carbon fabrics tested at a potential ranging from 0.01 to 3 V (a, b, c) and 1 to 3 V (d, e, f) after the cycles were compared. Figure 3c shows the rate performance of MoS_2/carbon fabrics at various current densities from 0.2 to 4 mA/cm^2 in a potential window of 1−3 V. When the current density increases to 4 mA/cm^2, the MoS_2/carbon fabric electrode still exhibits a high area capacity of 0.29 mAh/cm^2, and when returning back to 0.2 mA/cm^2, the capacity of MoS_2/carbon fabrics is recovered with a capacity retention of about 86.7%. The first two charge/discharge curves of pure carbon fabrics above 1 V are shown in Figure S3. As shown in Figure S3, pure carbon fabrics contribute a low area capacity of less than 0.015 mAh/cm^2 between 1 and 3 V. Figure 4a−c show the SEM images of MoS_2/carbon fabrics tested at a potential ranging from 0.01 to 3 V after 60 cycles, and it was observed that the structures of the carbon fabrics and graphene-like nanosheets were completely destroyed. The materials are partly peeled off from the carbon fabrics. Figure 4d−f show the SEM images of MoS_2/carbon fabrics tested at a potential ranging from 1 to 3 V after 400 cycles. Compared to the electrode that is tested at 0.01−3 V, the morphologies of MoS_2 were not destroyed completely, and thus we can see the nanosheet structure clearly.

2.3. Supercapacitor Performance. The MoS_2/carbon fabrics were also applied as self-standing electrodes of supercapacitors. The mass loading of MoS_2 on carbon fabrics used for SC tests is about 1.8−2.2 mg/cm^2. The capacitive properties of the MoS_2/carbon fabrics were first tested with cyclic voltammetry (CV) and galvanostatic charge−discharge measurements in three-electrode configurations. Figure 5a

DOI: 10.1021/acsomega.8b02446
ACS Omega 2018, 3, 17466−17473

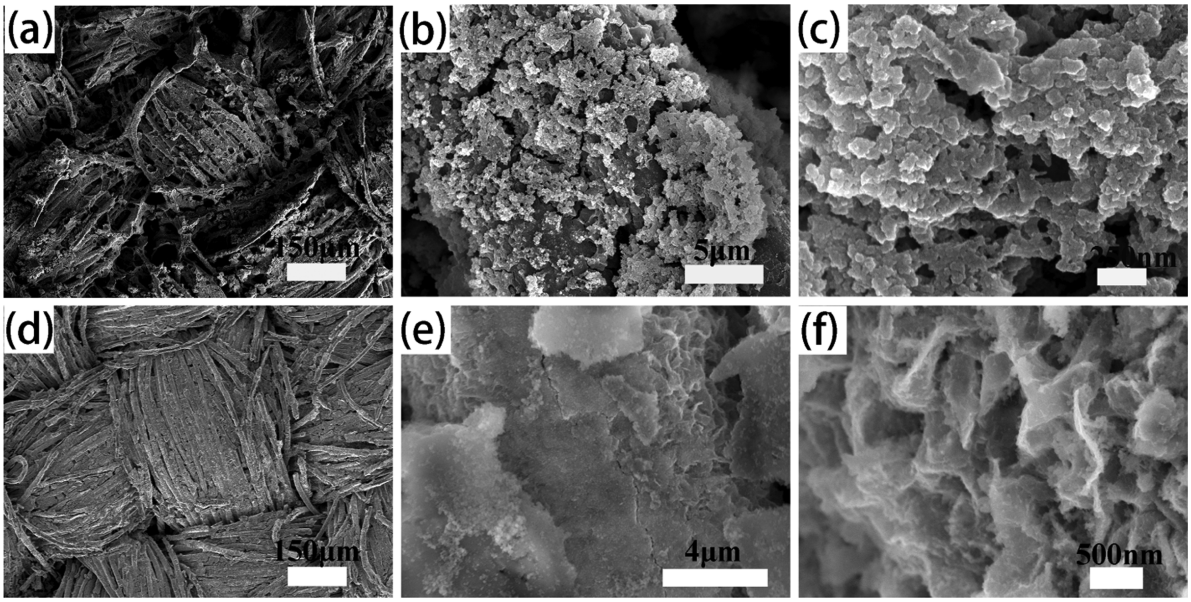

Figure 4. SEM images of the MoS_2/carbon fabric electrode after 60 cycles (a–c) and after 400 cycles (e, d, f). The charge/discharge potential range was 0.01–3 V (a–c) and 1–3 V (e, d, f), respectively.

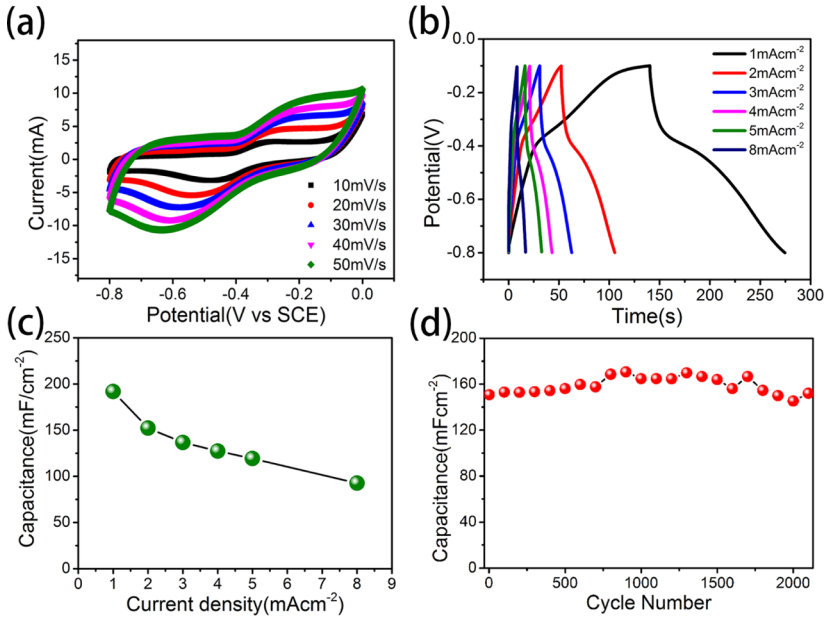

Figure 5. (a) CV curves, (b) constant-current charge–discharge voltage profiles, (c) specific capacitance as a function of current density, and (d) cycling performance at a current density of 2 mA/cm^2.

displays the CV curves of the MoS_2/carbon fabrics at scan speeds varying from 10 to 50 mV/s. The pseudocapacitance behavior can be confirmed obviously from the fact that the CV curve shape is different from the electrical double-layer capacitance, which is a nearly rectangular CV curve. Notably, redox peaks between −0.8 and 0 V can be seen in all CV curves due to the Faraday effect. As the scanning rate increases from 10 to 50 mV/s, the peak current rises up, but the CV curve shape shows no significant change. This result suggests that rapid redox reactions towards electrochemical energy storage can be performed with MoS_2/carbon fabrics.

Constant current charge/discharge profiles were conducted at current densities ranging from 1 to 8 mA/cm^2, which are displayed in Figure 5b. The representative capacitance of the electrode material is calculated as follows

$$C_{area} = I\Delta t/(\Delta VS)$$

where I represents the constant-discharge current, S means the geometrical area of the electrode, Δt is the discharged time after IR drop, and ΔV is the voltage drop upon discharge. The specific capacitance of the MoS_2/carbon fabric electrode calculated from each discharge curve is about 191.9, 152.3, 136.7, 127.4, 119.3, and 92.6 mF/cm^2 at 1, 2, 3, 4, 5, and 8 mA/cm^2, respectively, as shown in Figure 5c. Figure 5d shows the cycling performance of MoS_2/carbon fabrics at a current density of 2 mA/cm^2. After 2000 charge/discharge cycles, specific capacitance attenuation is negligible, indicating that

DOI: 10.1021/acsomega.8b02446
ACS Omega 2018, 3, 17466–17473

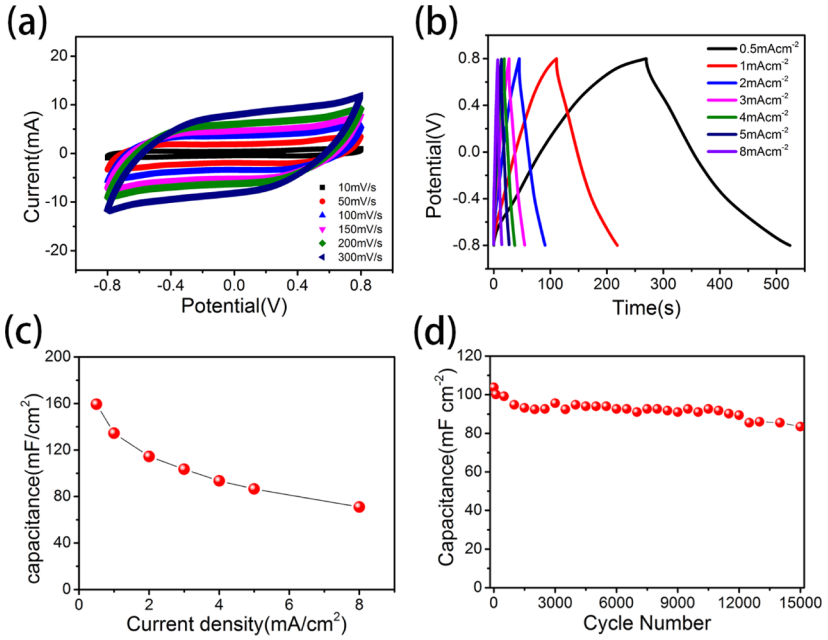

Figure 6. (a) CV curves, (b) constant-current charge−discharge voltage profiles, (c) specific capacitance as a function of current density, and (d) cycling performance at a current density of 3 mA/cm^2.

the MoS_2/carbon fabric electrode has superior cycling stability performance.

The symmetric two-electrode system adopted to evaluate the capacitive performance in this study due to the three-electrode configuration may easily overestimate the energy storage capability of an electrode material for practical supercapacitor use. Moreover, the cycling performance in a three-electrode system can be affected by some other aspects, such as the active materials peeling off from the current collectors. Figure 6a presents the CV curves of the two-electrode device at scan rates from 10 to 300 mV/s with a potential window between −0.8 and 0.8 V. Not only because of the surface electrosorption of Li^+ cations but also because of the fast, reversible successive surface redox reactions of MoS_2, the measured CV curves show quasirectangular shapes. It can be seen from the absence of redox peaks that the supercapacitor is charged and discharged at a pseudoconstant rate throughout the voltammetric cycle. From the galvanostatic charge−discharge measurements at current densities between 0.5 and 8 mA/cm^2, we obtained the accurate electrochemical values of the symmetric two-electrode system (Figure 6b). The capacitance of the electrode can be calculated according to the following equation

$$C_{area} = 2I\Delta t/(\Delta VS)$$

where I is the constant discharge current, S is the geometrical area of the electrode, Δt is the discharged time after IR drop, and ΔV is the voltage drop upon discharge, respectively.[39−41] The area capacitance values of the electrode were about 159.38, 134.5, 114.5, 103.5, 93.5, 85.63, and 71 mF/cm^2 at 0.5, 1, 2, 3, 4, 5, and 8 mA/cm^2 that are calculated from the charge/discharge curves, respectively, as shown in Figure 6c. Compared with the three-electrode configurations, the capacitance of the electrode is lower in a two-electrode system, which may be a normal phenomenon in the supercapacitor test. Figure 6d shows the cycling performance of the two-electrode system at 3 mA/cm^2. After 15 000 cycles, the electrode still retains a high specific capacitance of about 83.7 mF/cm^2 (about 80.6% capacitance retention).

3. CONCLUSIONS

In summary, graphene-like MoS_2 nanosheets have been successfully grown on carbon fiber fabrics with strong adhesion by a simple hydrothermal method. The MoS_2/carbon fabrics are self-standing electrodes for energy storage devices. When used as an anode for Li-ion batteries, graphene-like MoS_2/carbon fabrics give a high reversible area capacity of 0.5 mAh/cm^2, long cycling stability (80% capacity retention after 400 cycles), and excellent rate performance. A high specific capacitance of about 95 mF/cm^2 at 3 mA/cm^2 and extraordinary cycling stability (near 81% capacitance retention after 15 000 cycles) can be achieved as an electrochemical capacitor electrode. Because of the excellent cycling stability of MoS_2, we can composite with other electrode materials that have large specific capacitance but poor cycling stability to improve the electrochemical properties of electrode materials just like graphene and partly replace graphene in some special aspects.

4. METHODS

4.1. Materials Synthesis. Graphene-like MoS_2 nanosheets were obtained by a typical and simple hydrothermal method. Since all reagents used are analytical without further purification. To directly grow MoS_2 nanosheets on carbon fabrics, commercial carbon fabrics which are used as substrates were first cleaned with acetone, ethanol, and deionized water, and then the carbon fabrics were cut into the needed sizes (2 cm × 4 cm) and immersed in 0.5 M NaOH solution for about 1 h. After the above pretreatment, a piece of the above carbon fabrics was placed in a Teflon-lined stainless-steel autoclave (50 mL) containing a mixture of 0.3 g $Na_2MoO_4{\cdot}2H_2O$, 0.4 g CH_4N_2S, and 35 mL deionized water. The sealed autoclave was heated in an oven at 240 °C for 24 h. Immediately after the completion of the reaction, the reacted carbon cloth was

DOI: 10.1021/acsomega.8b02446
ACS Omega 2018, 3, 17466−17473

washed with deionized water and ethanol, and then dried in a vacuum oven at 80 °C for 12 h.

4.2. Characterization. The X-ray diffraction (XRD) pattern was obtained by using an X-ray diffractometer (X'Pert PRO, PANalytical B.V., the Netherlands) with Cu Kα radiation (λ = 0.154 nm). X-ray photoelectron spectrometry was performed on a VG Multi-lab 2000 system with a monochromatic Al Kα X-ray source. The morphologies and structures of the as-synthesized products were characterized by a field-emission scanning electron microscope (Nova NanoSEM 450, FEI, the Netherlands), a field-emission transmission electron microscope (Tecnai G2 F30, FEI, the Netherlands), and an atomic force microscope (AFM, SPM9700, Shimadzu).

4.3. Electrochemical Measurements. The carbon fabric-supported MoS_2 nanosheets directly acted as the working electrode. Lithium metal was used as the counter electrode, and a polypropylene film (Celgard-2300) was used as the separator. The electrolyte used was 1.0 M $LiPF_6$ solution with a mixture of ethylene carbonate and dimethyl carbonate (EC/DMC, 1:1 in volume). Galvanostatic charging and discharging tests were conducted using a battery testing system (Land, China) at a potential ranging from 1 to 3 V. The SC tests were performed on a CHI 660C electrochemical workstation in an aqueous LiOH electrolyte (1 M). The three-electrode cell tests were conducted with Pt foil as the counter electrode and a saturated calomel electrode as the reference electrode. The two-electrode SC tests were conducted in a two-electrode coin cell (CR2032) configuration assembled in air, where MoS_2/carbon fabrics serve as both the cathode and anode, glassy fibers serve as the separator. Coin cells were assembled in an argon-filled glovebox for a lithium-ion battery.

■ ASSOCIATED CONTENT

Supporting Information

The Supporting Information is available free of charge on the ACS Publications website at DOI: 10.1021/acsomega.8b02446.

Charge/discharge profiles of MoS_2/carbon fabrics; cycling performance of the MoS_2/carbon fabric electrode; and charge/discharge profiles of pure carbon fabrics (PDF)

■ AUTHOR INFORMATION

Corresponding Authors

*E-mail: chongli@hust.edu.cn (C.L.).
*E-mail: mqzhu@hust.edu.cn (M.-Q.Z.).

ORCID

Chong Li: 0000-0003-0453-2496
Ming-Qiang Zhu: 0000-0002-8886-4166

Author Contributions

‖H.Y. and Y.L. contributed equally to this work.

Notes

The authors declare no competing financial interest.

■ ACKNOWLEDGMENTS

This work was supported by the National Basic Research Program of China (Grant No. 2015CB755602, 2013CB922104), NSFC (51673077, 21474034, 51603078), the Fundamental Research Funds for the Central Universities (HUST: 2016YXMS029, HUST: 2018KFYXKJC033), and the Natural Science Foundation of Hubei Province (2018CFB574). We also thank the Analytical and Testing Center of Huazhong University of Science and Technology, the Center of Micro-Fabrication and Characterization (CMFC), and the Center for Nanoscale Characterization & Devices (CNCD) of WNLO for use of their facilities.

■ REFERENCES

(1) Mao, D.; Wan, J.; Wang, J.; Wang, D. Sequential Templating Approach: A Groundbreaking Strategy to Create Hollow Multishelled Structures. *Adv. Mater.* **2018**, No. e1802874.

(2) Qi, J.; Lai, X.; Wang, J.; Tang, H.; Ren, H.; Yang, Y.; Jin, Q.; Zhang, L.; Yu, R.; Ma, G.; Su, Z.; Zhao, H.; Wang, D. Multi-shelled hollow micro-/nanostructures. *Chem. Soc. Rev.* **2015**, *44*, 6749−6773.

(3) Wang, J. Y.; Tang, H. J.; Zhang, L. J.; Ren, H.; Yu, R. B.; Jin, Q.; Qi, J.; Mao, D.; Yang, M.; Wang, Y.; Liu, P. R.; Zhang, Y.; Wen, Y. R.; Gu, L.; Ma, G. H.; Su, Z. G.; Tang, Z. Y.; Zhao, H. J.; Wang, D. Multi-shelled metal oxides prepared via an anion-adsorption mechanism for lithium-ion batteries. *Nat. Energy* **2016**, *1*, No. 16050.

(4) Zhao, X.; Yu, R.; Tang, H.; Mao, D.; Qi, J.; Wang, B.; Zhang, Y.; Zhao, H.; Hu, W.; Wang, D. Formation of Septuple-Shelled $(Co_{2/3}Mn_{1/3})(Co_{5/6}Mn_{1/6})_2O_4$ Hollow Spheres as Electrode Material for Alkaline Rechargeable Battery. *Adv. Mater.* **2017**, *29*, No. 1700500.

(5) Ren, H.; Yu, R.; Wang, J.; Jin, Q.; Yang, M.; Mao, D.; Kisailus, D.; Zhao, H.; Wang, D. Multishelled TiO_2 Hollow Microspheres as Anodes with Superior Reversible Capacity for Lithium Ion Batteries. *Nano Lett.* **2014**, *14*, 6679−6684.

(6) Ren, H.; Sun, J.; Yu, R.; Yang, M.; Gu, L.; Liu, P.; Zhao, H.; Kisailus, D.; Wang, D. Controllable synthesis of mesostructures from TiO_2 hollow to porous nanospheres with superior rate performance for lithium ion batteries. *Chem. Sci.* **2016**, *7*, 793−798.

(7) Wang, J.; Tang, H.; Ren, H.; Yu, R.; Qi, J.; Mao, D.; Zhao, H.; Wang, D. pH-Regulated Synthesis of Multi-Shelled Manganese Oxide Hollow Microspheres as Supercapacitor Electrodes Using Carbonaceous Microspheres as Templates. *Adv. Sci.* **2014**, *1*, No. 1400011.

(8) Yin, H.; Cao, M. L.; Yu, X. X.; Li, C.; Shen, Y.; Zhu, M.-Q. Hierarchical $CuBi_2O_4$ microspheres as lithium-ion battery anodes with superior high-temperature electrochemical performance. *RSC Adv.* **2017**, *7*, 13250−13256.

(9) Li, H.; Ma, H.; Yang, M.; Wang, S.; Shao, H.; Wang, L.; Yu, R.; Wang, D. Highly controlled synthesis of multi-shelled NiO hollow microspheres for enhanced lithium storage properties. *Mater. Res. Bull.* **2017**, *87*, 224−229.

(10) Bao, W.; Liu, L.; Wang, C.; Choi, S.; Wang, D.; Wang, G. Facile Synthesis of Crumpled Nitrogen-Doped MXene Nanosheets as a New Sulfur Host for Lithium-Sulfur Batteries. *Adv. Energy Mater.* **2018**, *8*, No. 1702485.

(11) Li, D.; Zhao, X.; Yu, R.; Wang, B.; Wang, H.; Wang, D. Formation of multi-shelled nickel-based sulfide hollow spheres for rechargeable alkaline batteries. *Inorg. Chem. Front.* **2018**, *5*, 535−540.

(12) Wang, J.; Yang, N.; Tang, H.; Dong, Z.; Jin, Q.; Yang, M.; Kisailus, D.; Zhao, H.; Tang, Z.; Wang, D. Accurate Control of Multishelled Co_3O_4 Hollow Microspheres as High-Performance Anode Materials in Lithium-Ion Batteries. *Angew. Chem., Int. Ed.* **2013**, *52*, 6417−6420.

(13) Wang, J.; Cui, Y.; Wang, D. Design of Hollow Nanostructures for Energy Storage, Conversion and Production. *Adv. Mater.* **2018**, No. e1801993.

(14) Xu, S.; Hessel, C. M.; Ren, H.; Yu, R.; Jin, Q.; Yang, M.; Zhao, H.; Wang, D. alpha-Fe_2O_3 multi-shelled hollow microspheres for lithium ion battery anodes with superior capacity and charge retention. *Energy Environ. Sci.* **2014**, *7*, 632−637.

(15) Zhang, J.; Ren, H.; Wang, J.; Qi, J.; Yu, R.; Wang, D.; Liu, Y. Engineering of multi-shelled SnO_2 hollow microspheres for highly stable lithium-ion batteries. *J. Mater. Chem. A* **2016**, *4*, 17673−17677.

(16) Chen, K.; Zhang, T. S.; Huang, L. J.; Suo, Y. R.; Zhang, D. H.; Sun, J.; Wang, J. L. A facile and green synthesis of CDs-MoS_2-Fe_3O_4

DOI: 10.1021/acsomega.8b02446
ACS Omega 2018, 3, 17466−17473

nanohybrid for recyclable and enhanced photocatalysis in dye degradation. *Mater. Lett.* **2018**, *232*, 167−170.
(17) Xin, W. L.; Jiang, L. F.; Zong, L. P.; Zeng, H. B.; Shu, G. F.; Marks, R.; Zhang, X. J.; Shan, D. MoS_2 quantum dots-combined zirconium-metalloporphyrin frameworks: Synergistic effect on electron transfer and application for bioassay. *Sens. Actuators, B* **2018**, *273*, 566−573.
(18) Ren, X. P.; Wei, Q. B.; Ren, P. Y.; Wang, Y. H.; Chen, R. Synthesis of flower-like $MoSe_2$@MoS_2 nanocomposites as the high efficient water splitting electrocatalyst. *Mater. Lett.* **2018**, *231*, 213−216.
(19) Zhang, D. Z.; Jiang, C. X.; Wu, J. F. Layer-by-layer assembled In_2O_3 nanocubes/flower-like MoS_2 nanofilm for room temperature formaldehyde sensing. *Sens. Actuators, B* **2018**, *273*, 176−184.
(20) Yin, H.; Yu, X.-X.; Yu, Y.-W.; Cao, M.-L.; Zhao, H.; Li, C.; Zhu, M.-Q. Tellurium nanotubes grown on carbon fiber cloth as cathode for flexible all-solid-state lithium-tellurium batteries. *Electrochim. Acta* **2018**, *282*, 870−876.
(21) Yin, H.; Li, Q.; Cao, M.; Zhang, W.; Zhao, H.; Li, C.; Huo, K.; Zhu, M. Nanosized-bismuth-embedded 1D carbon nanofibers as high-performance anodes for lithium-ion and sodium-ion batteries. *Nano Res.* **2017**, *10*, 2156−2167.
(22) Yin, H.; Yu, X.; Li, Q.; Cao, M.; Zhang, W.; Zhao, H.; Zhu, M.-Q. Hollow porous CuO/C composite microcubes derived from metal-organic framework templates for highly reversible lithium-ion batteries. *J. Alloys Compd.* **2017**, *706*, 97−102.
(23) Yin, H.; Cao, M.; Yu, X.; Zhao, H.; Shen, Y.; Li, C.; Zhu, M.-Q. Self-standing Bi_2O_3 nanoparticles/carbon nanofiber hybrid films as a binder-free anode for flexible sodium-ion batteries. *Mater. Chem. Front.* **2017**, *1*, 1615−1621.
(24) Wang, J.; Tang, H.; Wang, H.; Yu, R.; Wang, D. Multi-shelled hollow micro-/nanostructures: promising platforms for lithium-ion batteries. *Mater. Chem. Front.* **2017**, *1*, 414−430.
(25) Du, J.; Qi, J.; Wang, D.; Tang, Z. Facile synthesis of Au@TiO_2 core-shell hollow spheres for dye-sensitized solar cells with remarkably improved efficiency. *Energy Environ. Sci.* **2012**, *5*, 6914−6918.
(26) Chen, M.; Wang, J.; Tang, H.; Yang, Y.; Wang, B.; Zhao, H.; Wang, D. Synthesis of multi-shelled MnO_2 hollow microspheres via an anion-adsorption process of hydrothermal intensification. *Inorg. Chem. Front.* **2016**, *3*, 1065−1070.
(27) Jiang, J.; Li, Y.; Liu, J.; Huang, X.; Yuan, C.; Lou, X. W. Recent Advances in Metal Oxide-based Electrode Architecture Design for Electrochemical Energy Storage. *Adv. Mater.* **2012**, *24*, 5166−5180.
(28) Liu, B.; Zhang, J.; Wang, X. F.; Chen, G.; Chen, D.; Zhou, C. W.; Shen, G. Z. Hierarchical Three-Dimensional $ZnCo_2O_4$ Nanowire Arrays/Carbon Cloth Anodes for a Novel Class of High-Performance Flexible Lithium-Ion Batteries. *Nano Lett.* **2012**, *12*, 3005−3011.
(29) Li, N.; Chen, Z. P.; Ren, W. C.; Li, F.; Cheng, H. M. Flexible graphene-based lithium ion batteries with ultrafast charge and discharge rates. *Proc. Natl. Acad. Sci. U.S.A.* **2012**, *109*, 17360−17365.
(30) Shen, L. F.; Che, Q.; Li, H. S.; Zhang, X. G. Mesoporous $NiCo_2O_4$ Nanowire Arrays Grown on Carbon Textiles as Binder-Free Flexible Electrodes for Energy Storage. *Adv. Funct. Mater.* **2014**, *24*, 2630−2637.
(31) Lu, X.; Zeng, Y. X.; Yu, M. H.; Zhai, T.; Liang, C. L.; Xie, S. L.; Balogun, M. S.; Tong, Y. X. Oxygen-Deficient Hematite Nanorods as High-Performance and Novel Negative Electrodes for Flexible Asymmetric Supercapacitors. *Adv. Mater.* **2014**, *26*, 3148−3155.
(32) Zhu, X. Q.; Liang, X. Y.; Fan, X. B.; Su, X. T. Fabrication of flower-like MoS_2/TiO_2 hybrid as an anode material for lithium ion batteries. *RSC Adv.* **2017**, *7*, 38119−38124.
(33) Xu, W.; Wang, T.; Yu, Y.; Wang, S. Synthesis of core-shell TiO_2@MoS_2 composites for lithium-ion battery anodes. *J. Alloys Compd.* **2016**, *689*, 460−467.
(34) He, J. R.; Li, P. J.; Lv, W. Q.; Wen, K. C.; Chen, Y. F.; Zhang, W. L.; Li, Y. R.; Qin, W.; He, W. D. Three-dimensional hierarchically structured aerogels constructed with layered MoS_2/graphene nanosheets as free-standing anodes for high-performance lithium ion batteries. *Electrochim. Acta* **2016**, *215*, 12−18.
(35) Zhu, J.; Sun, W. P.; Yang, D.; Zhang, Y.; Hoon, H. H.; Zhang, H.; Yan, Q. Y. Multifunctional Architectures Constructing of PANI Nanoneedle Arrays on MoS_2 Thin Nanosheets for High-Energy Supercapacitors. *Small* **2015**, *11*, 4123−4129.
(36) Hu, B. L.; Qin, X. Y.; Asiri, A. M.; Alamry, K. A.; Al-Youbi, A. O.; Sun, X. P. Synthesis of porous tubular C/MoS_2 nanocomposites and their application as a novel electrode material for supercapacitors with excellent cycling stability. *Electrochim. Acta* **2013**, *100*, 24−28.
(37) Gao, L. L.; Li, X. L.; Li, X. D.; Cheng, J. L.; Wang, B.; Wang, Z. Y.; Li, C. M. A coaxial yarn electrode based on hierarchical MoS_2 nanosheets/carbon fiber tows for flexible solid-state supercapacitors. *RSC Adv.* **2016**, *6*, 57190−57198.
(38) Baker, M. A.; Gilmore, R.; Lenardi, C.; Gissler, W. XPS investigation of preferential sputtering of S from MoS_2 and determination of MoS_x stoichiometry from Mo and S peak positions. *Appl. Surf. Sci.* **1999**, *150*, 255−262.
(39) Liu, Y.; He, X.; Hanlon, D.; Harvey, A.; Khan, U.; Li, Y.; Coleman, J. N. Electrical, Mechanical, and Capacity Percolation Leads to High-Performance MoS_2/Nanotube Composite Lithium Ion Battery Electrodes. *ACS Nano* **2016**, *10*, 5980−5990.
(40) Pan, Q.-c.; Huang, Y.-g.; Wang, H.-q.; Yang, G.-h.; Wang, L.-c.; Chen, J.; Zan, Y.-h.; Li, Q.-y. MoS_2/C nanosheets Encapsulated Sn@SnO_x nanoparticles as high-performance Lithium-ion battery anode material. *Electrochim. Acta* **2016**, *197*, 50−57.
(41) Geng, X.; Zhang, Y. L.; Han, Y.; Li, J. X.; Yang, L.; Benamara, M.; Chen, L.; Zhu, H. L. Two-Dimensional Water-Coupled Metallic MoS_2 with Nanochannels for Ultrafast Supercapacitors. *Nano Lett.* **2017**, *17*, 1825−1832.

DOI: 10.1021/acsomega.8b02446
ACS Omega 2018, 3, 17466−17473